

## CHANDRA DETECTION OF EXTENDED X-RAY EMISSION FROM THE RECURRENT NOVA RS OPHIUCHI

G. J. M. LUNA<sup>1</sup>, R. MONTEZ<sup>2</sup>, J. L. SOKOLOSKI<sup>3</sup>, K. MUKAI<sup>4</sup> AND J. H. KASTNER<sup>2</sup>

*Draft version September 26, 2018*

### ABSTRACT

Radio, infrared, and optical observations of the 2006 eruption of the symbiotic recurrent nova RS Ophiuchi (RS Oph) showed that the explosion produced non-spherical ejecta. Some of this ejected material was in the form of bipolar jets to the east and west of the central source. Here we describe X-ray observations taken with the *Chandra* X-ray Observatory one and a half years after the beginning of the outburst that reveal narrow, extended structure with a position angle of approximately 300 degrees (east of north). Although the orientation of the extended feature in the X-ray image is consistent with the readout direction of the CCD detector, extensive testing suggests that the feature is not an artifact. Assuming it is not an instrumental effect, the extended X-ray structure shows hot plasma stretching more than 1,900 AU from the central binary (taking a distance of 1.6 kpc). The X-ray emission is elongated in the northwest direction — in line with the extended infrared emission and some minor features in the published radio image. It is less consistent with the orientation of the radio jets and the main bipolar optical structure. Most of the photons in the extended X-ray structure have energies of less than 0.8 keV. If the extended X-ray feature was produced when the nova explosion occurred, then its  $1''.2$  length as of 2007 August implies that it expanded at an average rate of more than  $2 \text{ mas d}^{-1}$ , which corresponds to a flow speed of greater than 6,000 km/s ( $d/1.6 \text{ kpc}$ ) in the plane of the sky. This expansion rate is similar to the earliest measured expansion rates for the radio jets.

*Subject headings:* Binaries: symbiotic — stars: individual (RS Ophiuchi) — novae, cataclysmic variables — X-rays: binaries

### 1. INTRODUCTION

Novae are the most common major stellar explosions in the universe. The basic properties of these explosions are well explained by models in which a thermonuclear runaway at the base of the envelope of an accreting white dwarf (WD) causes the WD to brighten to near the Eddington luminosity and eject its envelope in a spherical outflow. An increasing number of observations, however, are indicating that the ejecta from many novae are anything but spherical (e.g., Slavin et al. 1995; Gill & O’Brien 2000; Krautter et al. 2002; Harman & O’Brien 2003), even in the X-rays (detected a century after outburst by Balman 2005). The properties of the outflows triggered by nova explosions on massive WDs are particularly important because they may influence or reveal the amount of mass lost per explosion, and thereby the ability of the stars to become type Ia supernovae.

Since the recurrence time for a nova explosion in a given system is inversely related to the mass of the WD (Yaron et al. 2005), interacting binaries that contain WDs with masses greater than approximately  $1.1 M_{\odot}$  can have recurrence times of less than 100 years; these systems are the so-called recurrent novae. In symbiotic recurrent novae — of which only 4 are known: RS

Oph, T CrB, V3890 Sgr and V745 Sco — the accreting WD is embedded in a dense nebula fed by the wind of the red-giant companion. RS Oph went into outburst for the sixth recorded time (previous outbursts occurred in 1898, 1933, 1958, 1967, 1985) on February 12th 2006 (Narumi et al. 2006). The astronomical community observed this outburst at virtually every wavelength; the X-ray range was extremely well covered, with observations by *RXTE* (Sokoloski et al. 2006), *Swift* (Hachisu et al. 2007; Bode et al. 2006), *Chandra*, and *XMM-Newton* (Ness et al. 2007; Nelson et al. 2008).

Observations of RS Oph indicate that the morphology of the expanding shell is complex and highly asymmetric. Within a few weeks of the start of the 2006 eruption, X-ray spectra showed that the blast-wave evolution deviated from self-similar, spherical expansion (Sokoloski et al. 2006; Bode et al. 2006). Bipolar structure along the east-west direction was clearly seen in radio images taken a few weeks into the 2006 outburst (O’Brien et al. 2006; Rupen et al. 2008); several months after the start of the outburst, observations showed that the radio jets were composed of highly collimated outflows that powered synchrotron-emitting lobes (Sokoloski et al. 2008). At optical wavelengths, [Ne V] $\lambda$ 3426 images 5 months after the start of the outburst revealed an expanding nebular remnant with a double-ring structure (Bode et al. 2007). The major axis of the double ring was also oriented east-west. Near infrared (NIR) interferometric observations also revealed extended asymmetric structure in the early expanding shell — but along a different direction. On day 5.5 after the start of the outburst, Chesneau et al. (2007) found

<sup>1</sup> Harvard-Smithsonian Center for Astrophysics, 60 Garden St. MS 15, Cambridge, MA, 02138, USA.

<sup>2</sup> 2100 Carlson Center for Imaging Science Rochester Institute of Technology Rochester, NY 14623 USA.

<sup>3</sup> Columbia Astrophysics Laboratory, 550 W. 220th Street, 1027 Pupin Hall, Columbia University, New York, NY 10027

<sup>4</sup> CRESST and X-ray Astrophysics Laboratory NASA/GSFC, Greenbelt, MD 20771, USA

that the NIR emission arose from a rapidly expanding elliptical region with major axis oriented from northwest to southeast. NIR observations in the first month of the outburst by Lane et al. (2007) also revealed an asymmetric structure with a position angle (P.A.) of approximately  $120^\circ/300^\circ$ .

In this letter, we describe the first detection of extended X-ray structure from RS Oph. Taken one and half years after the start of the 2006 eruption, our *Chandra* observations reveal a narrow X-ray feature along the direction of the NIR extended emission. We describe the observation in section §2, detail the analysis and results in section §3, and discuss possible interpretations of the results in section §4.

## 2. OBSERVATIONS

On 2007 August 4, the *Chandra* X-ray Observatory (CXO) observed RS Oph for 90.1 ks using the ACIS-S S3 back illuminated chip with a 1/4 subarray (ObsId 7457, start time 06:11:26 UT), in Timed Exposure mode and Faint telemetry format. The chip was read out every 0.94104 s, with the time between each read consisting of a 0.9 s exposure and 0.04104 s for charge transfer. RS Oph produced an average count rate of 0.0682 counts  $s^{-1}$ , or 0.0642 counts per frame integration time. The configuration we used ensured a minimal pile-up fraction (PIMMS<sup>5</sup> calculates a negligible pile-up fraction of 2%).

## 3. DATA ANALYSIS AND RESULTS

### 3.1. X-ray spectrum

With a source count rate of 0.0682  $c s^{-1}$  (see § 2), the background subtracted spectrum contained 6252 counts. The X-ray spectrum of RS Oph in quiescence is complex. Here we use a preliminary fit ( $\chi^2_\nu=1.35$  for 154 d.o.f.) consisting of two soft, relatively unabsorbed thermal plasma components (*mekal*) and a hard, heavily absorbed cooling flow (*mkcflow*) component (using the model names found in XSPEC; Arnaud et al. 1996). This fit adequately models the observed spectrum for the purposes of the PSF deconvolution processes. We will present a full analysis and interpretation of the spectrum in a forthcoming paper (Nelson et al. in preparation).

### 3.2. Extended X-ray structure

Since observations at other wavelengths suggested that any extended structure would be on the order of an arcsec in length, we applied a Subpixel Event Repositioning (SER; Li et al. 2003, 2004) technique to obtain the best possible spatial resolution. On the basis of a physical model of the photon-CCD interaction, SER uses the available information concerning photon event charge splitting to reconstruct the most likely entrance positions of photons within individual CCD pixels. This procedure potentially improves the effective *Chandra*/ACIS pixel size from  $0''.5$  to as small as  $0''.3$ , albeit with a non-uniform shape and a strong dependence on event charge split (i.e., event grade); see Li et al. (2003) for details. Due to the significant number of counts detected, we used a spatial bin size of  $0''.125$  in constructing the X-ray images analyzed here, so as to make best use of the potential improvement in spatial resolution afforded

by SER. After applying SER, we performed a maximum likelihood deconvolution on the image using a synthetic Point Spread Function (PSF) appropriate for the source off-axis angle and X-ray spectrum. Altogether, the process for generating the final image consisted of the following steps: 1) extract and fit the spectrum; 2) use the *Chandra* Ray Tracer (ChaRT; Carter et al. 2003), with the spectral model from #1, to trace the rays through the *Chandra* X-ray optics, and then use MARX (Model of AXAF Response to X-rays) to project those rays onto the detector and create a synthetic PSF 3) apply SER to the pipeline-processed event file; 4) use the synthetic PSF from step #2 and the SER-processed event file from step #3 to perform maximum likelihood deconvolution.

The maximum likelihood deconvolution of the *Chandra* observation reveals a feature extending northwest of the central binary ( $\alpha=17^h 50^m 13.2s$ ,  $\delta=-06^\circ 42' 28.2''$ ) at a P.A. (east of north) of approximately  $300^\circ$  (Fig. 1 and 2). The length of the extended feature, as measured from the centroid of the central X-ray emission to the location where the intensity falls below 10 counts per  $0''.125$  pixel, is  $1.2\pm 0.3$  arcsec. We took the uncertainty on the length of the extended structure to be the best achievable SER pixel size, i.e.,  $0''.3$ . A comparison among images from four different energy bands (selected to contain roughly 1,000 counts each) showed that the narrow X-ray feature is primarily composed of photons with energies less than about 0.8 keV (see Fig. 3).

### 3.3. Tests of the extended X-ray structure

Although the X-ray feature lies along the readout direction of the CCD, extensive testing supports our conclusion that it is not an artifact but is instead representative of the actual X-ray morphology of RS Oph. Any excess charge from a readout artifact would appear as a string of spurious X-ray events which, for bright sources (*Chandra* POG v.11), are not removed by standard grade filtering and fall along rows of pixels with constant y-coordinate in the CCD pixels array (CHIPY). Readout streaks are therefore always symmetric and might appear along pixels with the same CHIPY value as the source. Fig. 1 shows that the detected X-ray feature is not symmetric with respect to the central source. Furthermore, any readout artifact in the region of the CCD where we detect the feature would account for only a few counts, whereas we detect  $\sim 100$  counts in the  $\sim 1''.2$  X-ray feature; we therefore conclude that it is not due to a readout artifact.

Charge Transfer Inefficiency (CTI) in the S3 chip changes the overall instrument performance in various ways. First, since some charge is trapped, the charge read out is less than the amount of charge deposited. Second, CTI causes a migration of the grades assigned to each event due to photons that were captured by the traps and gradually *re-emitted* in the following frames. This second effect can change grades from that associated with a single pixel events (flight grade = 0) to those associated with a vertical up-split (flight grades = 2, 66), which are oriented parallel to the readout direction (R. Edgars, private communication). Since no tested CTI-correction algorithm is available for observations taken in subarray mode, we performed several tests to indicate the degree to which our observation was affected by

<sup>5</sup> <http://heasarc.nasa.gov/docs/software/tools/pimms.html>

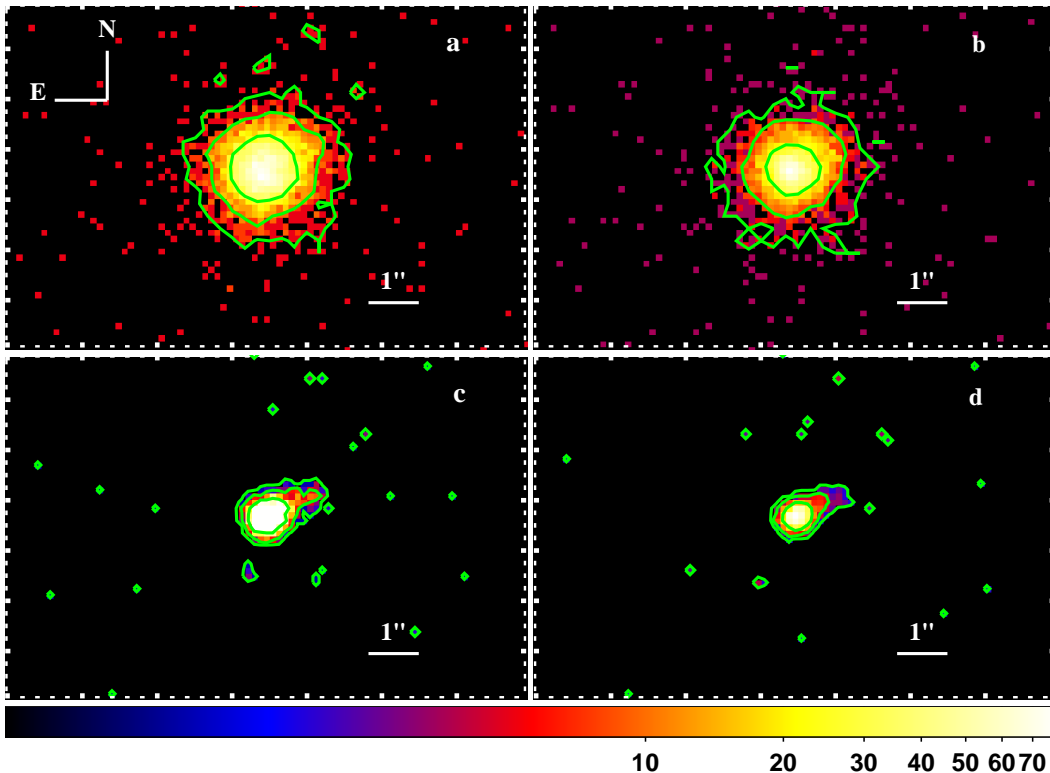


FIG. 1.— Comparison of *Chandra* images of RS Oph with various levels of image processing. (a) Image obtained from pipeline products without further processing; (b) Image created after applying Subpixel Event Repositioning (SER, see text) to the data; (c) Resulting image after performing maximum likelihood deconvolution using a simulated PSF; (d) Image created after applying both SER and maximum likelihood PSF deconvolution as described in §3.2. A comparison of panels (a) and (b) confirms that SER does not introduce any spurious asymmetry into the image. A comparison of panels (c) and (d) shows that the extended structure was clearly visible in the deconvolved image, even before the application of SER. The innermost contour encloses 4095, 3739, 4955, and 5140 counts in panels (a) through (d), respectively. Between the innermost and middle contours are 1252, 1589, 649, and 489 counts for panels (a) through (d), respectively. Between the middle and outermost contours are 299, 326, 66, and 64 counts for panels (a) through (d), respectively. North is up and east is to the left.

CTI<sup>6</sup>.

The S3 back-illuminated (BI) chip has substantial CTI in the serial array. If severe, this can create an extended feature in the direction along which the charges move out of the frame store region. In our observation, such an effect would correspond to a feature aligned in a direction *perpendicular* to the one we detected. On the other hand, the detected feature could be caused by parallel CTI. To investigate the presence of parallel CTI, we applied our image processing procedure to an observation from the *Chandra* archive that was taken with the same instrumental configuration (see § 2) and has roughly the same count rate as our observation. The observation we used was of HD113703 B (ObsID 626, exposure time = 12.7 ks). Trapped charges are unlikely to be re-emitted as grade-0 events. Since the narrow extended structure from RS Oph appeared strongly when we created an image using only grade 0 events, we examined an image of HD113703 B created using only grade 0 events. The grade-0 image of HD113703 B did not show any extended structure along the read out direction. This last test suggests that CTI effects were absent.

We also carefully tested whether the image processing that we performed could have introduced the detected

feature as an artifact. SER is a event-by-event procedure that should not reposition the events in a preferential direction. Nevertheless, to confirm that SER did not introduce an artifact, we applied the deconvolution procedure to data with and without SER applied (see Fig. 1). No significant differences were found between the SER and non-SER deconvolved images. We therefore conclude that the narrow X-ray feature was not a by-product of applying SER. If the synthetic PSF was not symmetric, the deconvolution could have introduced artifacts in the resulting image. To test for this possibility, we applied the deconvolution with various rotations and flips of the PSF with no significant changes in the orientation of the extended feature. Finally, as we discuss below, features at roughly the same P.A. as the extended X-ray feature have been seen in radio and IR observations of RS Oph.

#### 4. DISCUSSION AND CONCLUSION

Assuming, as suggested by our extensive testing, that the extended X-ray structure is not an artifact, the properties of this feature indicate that it consists of a few tenths of a percent to a few percent of the ejecta mass, and that the outermost X-ray emitting material is moving at a speed approximately half of the escape velocity from the WD (the escape velocity is approximately 12,600 km s<sup>-1</sup> for a 1.35 M<sub>⊙</sub> WD). If the material com-

<sup>6</sup> The CTI correction applied by the standard pipeline process was removed before performing any tests.

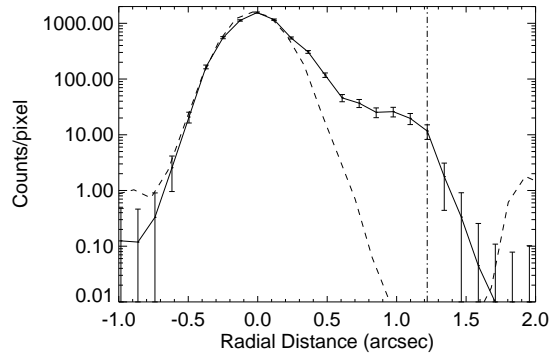


FIG. 2.— Profiles of the intensity along, and perpendicular to, the narrow X-ray feature. The solid curve shows the intensity profile along the narrow feature while the dotted line shows the profile in the direction perpendicular to the feature. The length of the extended feature, as measured from the centroid of the PSF to the location where the intensity falls below 10 counts per  $0''.125$  spatial bin (marked with a dot-dashed vertical line), is  $1.2 \pm 0.3$  arcsec. Error bars represent one standard deviation. The error in radial distance was estimated to be the best achievable SER pixel size, i.e.,  $0''.3$ .

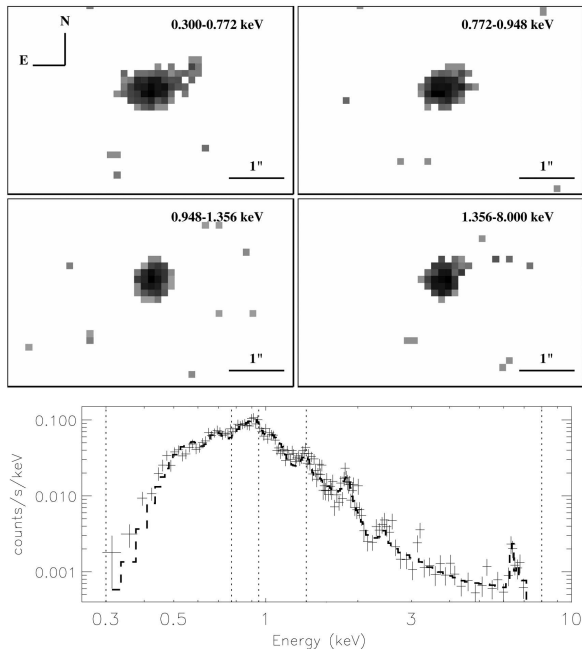


FIG. 3.— Images (to which both SER and maximum likelihood deconvolution have been applied) in 4 energy bands containing roughly the same number of counts (1000). Lower panel: *Chandra* spectrum of RS Oph (and overlaid best-fit model) with dashed vertical lines indicating the 4 energy ranges used to generate the 4 images in the upper panels. The asymmetric X-ray feature is most pronounced in the soft band ( $E < 0.77$  keV).

prising the narrow X-ray feature was ejected at the time of the nova explosion, the length of the X-ray structure suggests an average expansion rate in the plane of the sky of  $\sim 2.3$  mas  $d^{-1}$ . This rate is similar to the early expansion rate of  $\sim 2$  mas  $d^{-1}$  for the radio jet (Sokoloski et al. 2008). The rate of expansion of the X-ray feature corresponds to velocities in the plane of the sky of about  $\sim 6,300 \pm 1600$  km  $s^{-1}$  ( $d/1.6$  kpc). Since the X-ray

emitting material is unlikely to be moving exactly in the plane of the sky, the true velocity could be higher.

A strong shock moving at such a high speed would be expected to produce hard X-ray emission (with  $kT \simeq 40$  keV in the strong-shock case); however we find only soft X-ray emission from the extended feature (§3.2). The discrepancy between the expected temperature in the strong shock case and the observed photon energy is also present in the diffuse X-ray emission from planetary nebulae (Soker & Kastner 2003) and the two symbiotic stars with X-ray jets – CH Cyg (Galloway & Sokoloski 2004) and R Aqr (Kellogg et al. 2007).

The narrow X-ray feature is most extended in the 0.3–0.8 keV energy band and contains approximately 40 photons in this band. A crude estimation of its mass can be made if we assume that the emission is due to an absorbed, optically thin thermal plasma with  $kT=0.5$  keV and  $n_H=1.8 \times 10^{21}$   $cm^{-2}$  (Bode et al. 2006). We use PIMMS to obtain the observed emission measure of such a plasma and, assuming that the narrow X-ray feature has a radius of  $\sim 0''.9$  and length of  $1''.2$  (Fig. 2), find that the density is  $\sim 40$   $cm^{-3}$  and the mass of the extended X-ray emitting material is  $\sim 10^{-8}$   $M_\odot$  (assuming that there is one proton for every free electron). For comparison, estimates of the amount of material ejected immediately after the outburst range from  $\sim 10^{-7}$   $M_\odot$  to  $\sim 10^{-6}$   $M_\odot$  (Sokoloski et al. 2006; Hachisu et al. 2007).

The orientation of the narrow X-ray feature is less consistent with that of the radio jets (O’Brien et al. 2006; Rupen et al. 2008; Sokoloski et al. 2008) than with other features detected at radio and infrared (NIR) wavelengths. Early radio observations showed that the ring of synchrotron-emitting plasma associated with the expanding blast wave had a bright spot at a P.A.  $\approx 120^\circ$  (O’Brien et al. 2006; Rupen et al. 2008). If one were to superpose the X-ray and radio images and draw a line along the extended X-ray structure, it would intersect the bright spots on the radio ring. Moreover, the radio ring was actually more of a C-shape, with the opening in the ring at the same P.A. as the X-ray feature. NIR interferometry uncovered extended emission with a P.A. of  $120^\circ/300^\circ$  from day 5.5 to a few months after the nova explosions (Chesneau et al. 2007; Lane et al. 2007), and Chesneau et al. (2007) suggested a possible connection between the radio and IR morphologies. Our detection of an X-ray feature extending in the northwest direction, like features in the radio and NIR, suggests that the structures along this direction could all be related (see Fig. 4).

Although the X-ray structure has some similarities to features predicted by models of the explosion, many properties of the observed narrow X-ray feature are unexplained, and the true origin of this extended X-ray emitting gas remains unclear. Computational modeling suggests that the blast-wave expansion should be strongly asymmetric. For example, in the 3-dimensional simulations of Walder et al. (2008), the blastwave moves into a highly inhomogeneous pre-outburst density distribution and forms an elongated, bipolar structure perpendicular to the plane of the orbit. We do not see any extended X-ray emission in this direction. In contrast, models by Orlando et al. (2009) predict a one-sided X-ray structure – as we have found – due to the reflection of the blastwave

off of the red giant. Unfortunately, however, the position of the red giant at the time of the nova explosion (according to the ephemeris of Brandi et al. 2009) would have led to an X-ray extension in the north-south direction, which is inconsistent with our detection of extended X-ray emission at a P.A. of 300 degrees. Thus, our results suggest that either the orbital solution for this system needs to be re-examined or that the explosion somehow ejected X-ray emitting plasma in a direction that was neither perpendicular to the plane of the orbit nor along the line joining the WD and the red giant.

We thank L. Townsley, F. Bauer, E. Gotthelf, R. Edgars, and M. McCollough for discussions about the ACIS CCDs, T. Nelson for discussion about spectral results, and O. Chesneau for providing us a good quality version of Fig. 4b. Support for this work was provided by NASA through Chandra awards GO7-8030X and GO6-7022A issued by the Chandra X-ray Observatory Center, which is operated by the SAO for and on behalf of NASA under contract NAS8-03060.

*Facilities:* CXO (ASIS).

#### REFERENCES

- Arnaud, K.A., 1996, *Astronomical Data Analysis Software and Systems V*, eds. Jacoby G. and Barnes J., p17, ASP Conf. Series volume 101.
- Balman, S., 2005, *ApJ*, 627, 933
- Bode, M.F., O'Brien, T.J., Osborne, J.P., Page, K.L., Senziani, F., et al., 2006, *ApJ*, 652, 629
- Bode, M. F., Harman, D. J., O'Brien, T. J., Bond, H. E., Starrfield, S., Darnley, M. J., Evans, A. & Eyres, S. P. S., *ApJ*, 2007, 665, L63
- Brandi, E.; Quiroga, C.; Mikolajewska, J.; Ferrer, O. E.; Garcia, L. G., 2009, *astro-ph...*
- Chesneau, O., Nardetto, N., Millour, F., Hummel, C., et al., 2007, *A&A*, 464, 119
- Carter, C., et al., 2003, *ADASS XII ASP Conference Series*, 295, 477
- Galloway, D. K. & Sokoloski, J. L., 2004, *ApJ*, 613, 61
- Gill, C. D., & O'Brien, T. J., 2000, *MNRAS*, 314, 175
- Hachisu, I., Kato, M. & Luna, G. J. M., 2007, *ApJ*, 659, 153
- Harman, D. J., & O'Brien, T. J., 2003, *MNRAS*, 344, 1219
- Kellogg, E., Anderson, C., Korreck, K., DePasquale, J., Nichols, J., Sokoloski, J. L., Krauss, M., Pedelty, J., 2007, *ApJ*, 664, 1079
- Krautter, J., Woodward, C. E., Schuster, M. T. et al., 2002, *ApJ*, 124, 2888
- Lane, B. F., Sokoloski, J. L., Barry, R. K., Traub, W. A., Retter, A., et al., 2007, *ApJ*, 658, 520
- Li, J., Kastner, J. H., Prigozhin, G. Y., Schulz, N. S., 2003, *ApJ*, 590, 586
- Li, J., Kastner, J. H., Prigozhin, G. Y., Schulz, N. S., Feigelson, E. D. & Konstantin, G. V., 2004, *ApJ*, 610, 1204
- Narumi, H., Hirosawa, K., Kanai, K., Renz, W. et al., 2006, *IAU Circ.*, 8671, 2
- Nelson, T., Orio, M., Cassinelli, J. P., Still, M., Leibowitz, E., Mucciarelli, P., 2008, *ApJ*, 673, 1067
- Ness, J.-U., Starrfield, S., Beardmore, A.P., Bode, M.F., Drake, J.J., et al., 2007, *ApJ*, 665, 1334
- O'Brien, T. J., Bode, M. F., Porcas, R. W., Muxlow, T. W. B., S. P. S., et al., *Nature*, 442, 279
- Orlando, S., Drake, J. J. & Laming, J. M., 2009, *A&A*, 493, 1049
- Rupen M. P., Miodusaewski, A. J. & Sokoloski, J. L., 2008, *ApJ*, 688, 559
- Slavin, A. J., O'Brien, T. J., & Dunlop, J. S. 1995, *MNRAS*, 276, 353
- Soker, N. & Kastner, J. H., 2003, *ApJ*, 583, 368
- Sokoloski, J. L. Luna, G. J. M., Mukai, K. & Kenyon, S. J., *Nature*, 442, 276
- Sokoloski, J. L., Rupen, M. P. & Mioduszewski, A. J., 2008, *ApJ*, 685, L137
- Walder, R., Folini, D. & Shore, S. N., 2008, *A&A*, 484, 9
- Yaron, O., Prialnik, D., Shara, M. M., Kovetz, A., 2005, *ApJ*, 623, 398

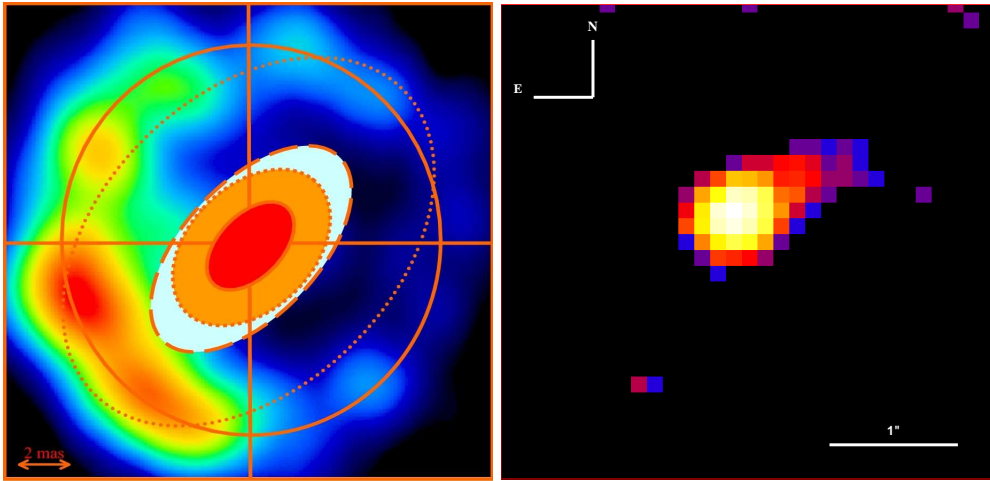


FIG. 4.— Comparison of RS Oph images in radio, infrared and X-rays. *Left*: an image of radio synchrotron-emitting plasma with NIR contours overlaid (Chesneau et al. 2007). *Right*: the X-ray image obtained after SER and PSF-deconvolution processing (same as panel (d) in Fig. 1). The X-ray feature extends along the same direction as the NIR and radio features, suggesting that they could all be related. Note that the two panels show very different scales.